SCIENTIFIC REPORTS

OPEN

SUBJECT AREAS:
CELLULAR NEUROSCIENCE
GENETICS OF THE NERVOUS SYSTEM
NEURAL PROGENITORS
GENETIC VECTORS

Received
9 January 2013

Accepted
6 March 2013

Published
21 March 2013

Correspondence and requests for materials should be addressed to J.L. (julia.ledderose@mpimf-heidelberg.mpg.de) or M.K.S. (martin.schwarz@mpimf-heidelberg.mpg.de)

Maturation of postnatally generated olfactory bulb granule cells depends on functional γ-protocadherin expression

Julia Ledderose, Sandra Dieter & Martin K. Schwarz

Max Planck Institute for Medical Research, Jahnstr. 29, 69120 Heidelberg, Germany.

γ-protocadherins (γ-pcdhs) are transmembrane receptor proteins ubiquitously expressed in the postnatal and adult mouse brain. γ-pcdhs are required for normal neuronal development as shown for spinal cord interneurons, retinal ganglion cells and cortical neurons. To test the role of γ-pcdhs during development of subventricular zone progenitor cells and their subsequent differentiation into olfactory granule cells we generated a conditional γ-pcdh$^{lox/lox}$ allele (γ-pcdh$^{lox/lox}$) allowing for functional γ-pcdh inactivation upon lentivirus-mediated Cre-recombinase expression selectively in subventricular zone progenitor cells. While γ-pcdh loss did not alter the proliferation of subventricular zone progenitors, γ-pcdh ko progenitors that reached the main olfactory bulb showed a significant reduction in dendritic arborization and failed to develop dendritic spines. Our results suggest that olfactory bulb granule cell maturation necessitates functional γ-pcdh expression.

γ-protocadherins (γ-pcdhs) belong to the cadherin super-family and are arranged with α- and beta-protocadherins in three tandemly arrayed gene clusters on mouse chromosome 18[1]. γ-pcdhs encode transmembrane proteins, which may contribute to the complex wiring of the nervous system[1,2]. In the vertebrate central nervous system, γ-pcdhs are expressed in diverse neuronal populations. α- and γ-pcdhs are enriched in the postsynaptic density of synapses forming hetero-protein complexes[3,4]. γ-pcdhs are subject to matrix metallo-protease (MMP) cleavage and presenilin-dependent intramembrane proteolysis. MMP-mediated shedding of the ectodomain and subsequent release of the cytoplasmic domain by the γ-secretase complex results in translocation of the intracellular domain into the nucleus and transcriptional activation of target genes[5,6]. Conditional deletion of all 22 γ-pcdh genes from the mouse γ-pcdh cluster affects development of multiple neuronal types such as retinal ganglion cells and spinal cord interneurons, leading to decreased synapse numbers and increased neuronal apoptosis[7,8]. In the spinal cord the increase in neuronal apoptosis was regarded as consequence of reduced synapse numbers, as blocking of apoptosis by deleting the proapoptotic protein Bax in γ-pcdh ko mice still led to a reduction in synapse numbers[7]. This result is consistent with the idea that failure of synapse formation or function impairs neuronal survival[9]. In contrast, deletion of γ-pcdhs in the Bax$^{-/-}$ background did not decrease synapse density in the retina[8], making it unlikely that apoptosis reflects an elimination of synapses. In summary, in the spinal cord synapses are lost in the absence of apoptosis, whereas in the retina neurons are lost in the absence of major synaptic defects. Recently it was reported that γ-pcdh ablation in cortical neurons resulted in aberrant dendrite arborization, while synaptic density and neuronal survival were unaffected[10]. Together, these findings suggest distinct, brain region dependent mechanisms of γ-pcdhs in neuronal differentiation, synapse formation and survival.

In the mammalian subventricular zone (SVZ), neurogenesis is ongoing throughout adult life[11]. Undifferentiated neural B-type stem cells, characterized by expression of glial fibrillary acidic protein (GFAP), generate Doublecortin (Dcx) expressing A-type neuroblasts via transit-amplifying C-type progenitors[12,13]. Newly born A-type neuroblasts migrate from the SVZ along the rostral migratory stream (RMS) into the main olfactory bulb (OB) where they differentiate into axonless olfactory granule cells (GC), or periglomerular cells[14]. Newborn neuroblasts traced by [3H]-thymidine[15] are categorized according to their morphology into five different stages, beginning from precursor cells in the RMS (Stage 1) to maturated and differentiated GCs in the OB (Stage 5). Labeling of SVZ progenitors by retroviral injections into the SVZ showed that synaptogenesis starts at soma and basal dendrites of olfactory GCs ~10 days after injection[16,17].

In this study we accessed SVZ progenitor cells by LV-mediated infection and investigated the fate of γ-pcdh ko neuroblasts after Cre-recombinase-mediated recombination in γ-pcdh$^{lox/lox}$ mice. This experimental setup

allowed us to study the differentiation and maturation of "floxed" γ-pcdh ko progenitors in the postnatal brain. Our conditional γ-pcdh$^{lox/lox}$ allele overcame neonatal lethality and switched off functional γ-pcdh expression specifically in SVZ A-, B-, and C-type cells. We found that LV-infected γ-pcdh ko progenitors developed into Dcx positive, A-type neuroblasts, migrating along the RMS and populating the OB. γ-pcdh-deficient progenitors in the OB started to differentiate into GCs with marked impairments in dendrite arborization and spine formation as demonstrated by Sholl analysis. Our results indicate that functional γ-pcdh expression is important for the proper maturation and differentiation of postnatally born olfactory GCs.

Results

Lentivirus-mediated conditional γ-pcdh ko of SVZ progenitor cells. The SVZ constantly generates neuronal progenitors populating the main olfactory bulb (OB) where they differentiate into mature olfactory granule cells (GC) and periglomerular cells. This ongoing neurogenesis offers the unique possibility to study the fate of a neuron from its progenitor stage in the SVZ up to its mature stage as a fully differentiated functionally integrated GC in the OB[18]. Since γ-pcdhs are ubiquitously expressed in the SVZ of perinatal and adult mice[3,19,20] (Fig. S1), we used this model system to study their function during neuronal migration, differentiation, and maturation via region-specific conditional deletion of γ-pcdhs in SVZ stem cells. For this purpose, and because γ-pcdh kos are not viable for more than ~3 hours after birth, we generated a conditional γ-pcdh ko allele (γ-pcdh$^{lox/lox}$) to allow region-specific γ-pcdh deletion in perinatal as well as adult mice (Fig. 1A and Methods). Western blot analysis for γ-pcdhs from brain lysates of these "floxed" mice showed no difference in γ-pcdh expression levels between γ-pcdh$^{lox/lox}$ and wt littermates, indicating correct γ-pcdh expression in floxed mice. No signal was detected in the complete ko at P0[5] (Fig. 1B).

To induce conditional γ-pcdh deletion in SVZ progenitors we constructed a lentivirus (LV) expressing Cre recombinase linked with an internal ribosomal entry site (IRES) to EGFP (LV-Cre-EGFP), under the control of an ubiquitin promoter/enhancer element (see Fig. 2A and Methods). LVs have been shown to stably infect both, dividing and non-dividing cells and can be efficiently used for infection of different types of progenitor cells in the SVZ[21–23].

We next tested the time that is required for LV expressed Cre recombinase to ablate functional γ-pcdh expression after infection. We found that LV injection of LV-Cre-EGFP into the lateral ventricles of neonatal and adult Rosa26 reporter mice[24] induced functional Cre expression in SVZ progenitors as early as 24 hours after virus delivery shown by analysis of beta-galactosidase activity from 1 to 14 dpi (Fig. S2).

To test possible effects on cell survival after Cre over-expression in wt SVZ progenitor cells, we next stereotaxically injected a cocktail of LV-Cre-EGFP together with a LV, expressing the fluorescent protein tdTomato (LV-tdTom, ratio 1 : 1) into the SVZ of neonatal (at P0) and adult wt mice (Fig. 2A). Subsequent analysis by immunolabeling at 4, 6, 10, 14, and 31 dpi revealed no morphological differences between EGFP positive (EGFP$^+$) and tdTomato positive (Tom$^+$) cells in the SVZ (shown for 4, 6, and 10 dpi, Fig. 2B–D). Counting of EGFP$^+$ and Tom$^+$ cells in the SVZ at the analyzed stages showed no significant differences in numbers (Fig. 2E, Table S1, Student's t-test, $p < 0.05$, ANOVA, $p < 0.001$, $n = 3$ mice per stage, 3–6 brain sections per mouse). As expected for LV infections, the number of EGFP$^+$/Tom$^+$ double-positive cells analyzed at 4, 6, 10, 14 and 31 dpi in the SVZ as well as in the OB (Table S1, Fig. 2E, $n = 3$ mice per stage, 4–6 brain sections per mice) was very low and therefore not included in our calculations. To demonstrate that our virus cocktail injections reliably resulted in comparable infection efficacies of both

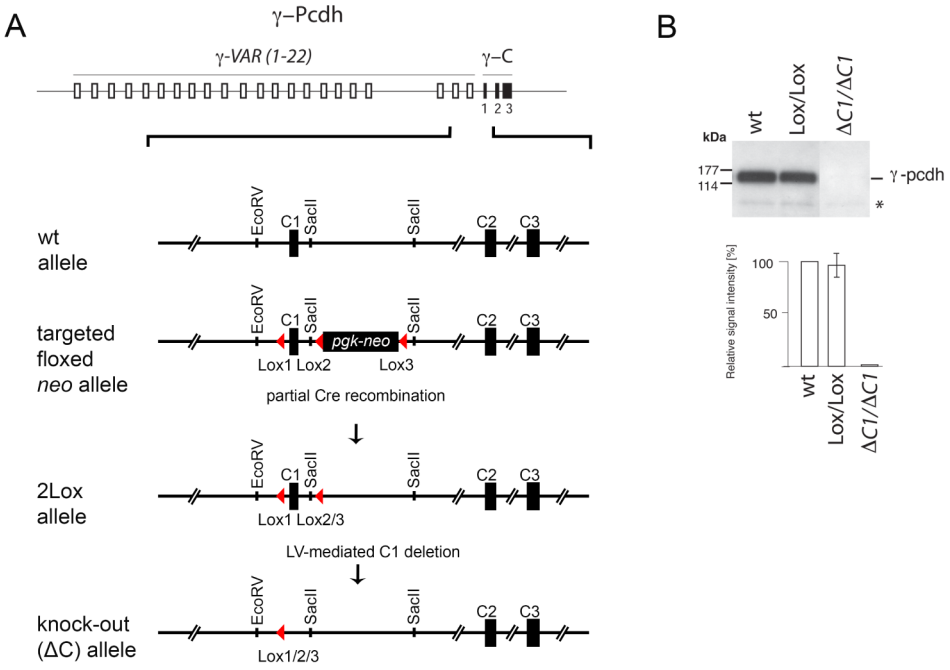

Figure 1 | Conditional ko of the γ-pcdh locus. (A) A viable conditional ko allele of the γ-pcdh gene cluster was generated by insertion of two LoxP sites on each side of constant region exon γ-*C1*. The schematic drawing shows the γ-pcdh locus with the 22 variable region exons (open boxes) and the three constant region exons (γ-*C1* to *C3*, black boxes). The close-up below shows the wt allele and the targeted 3Lox allele containing the floxed lethal *pgk-neo* cassette. The floxed 2Lox allele containing two LoxP sites was obtained after excision of the *pgk-neo* cassette by crossings with EIIaCre mice. A functional γ-pcdh ko can subsequently be generated by Cre-mediated excision of "floxed" γ-*C1*. (B) Western blot analysis for γ-pcdh in wt, "floxed" (Lox/Lox), and γ-pcdh ko (Δ*C1*/Δ*C1*) mice. Quantification of western blots revealed no differences in γ-pcdh expression between wt and γ-pcdh$^{lox/lox}$ mice (relative signal intensity [%]), whereas in γ-pcdh ko mice no signal was detected (the asterisk marks unspecific bands).

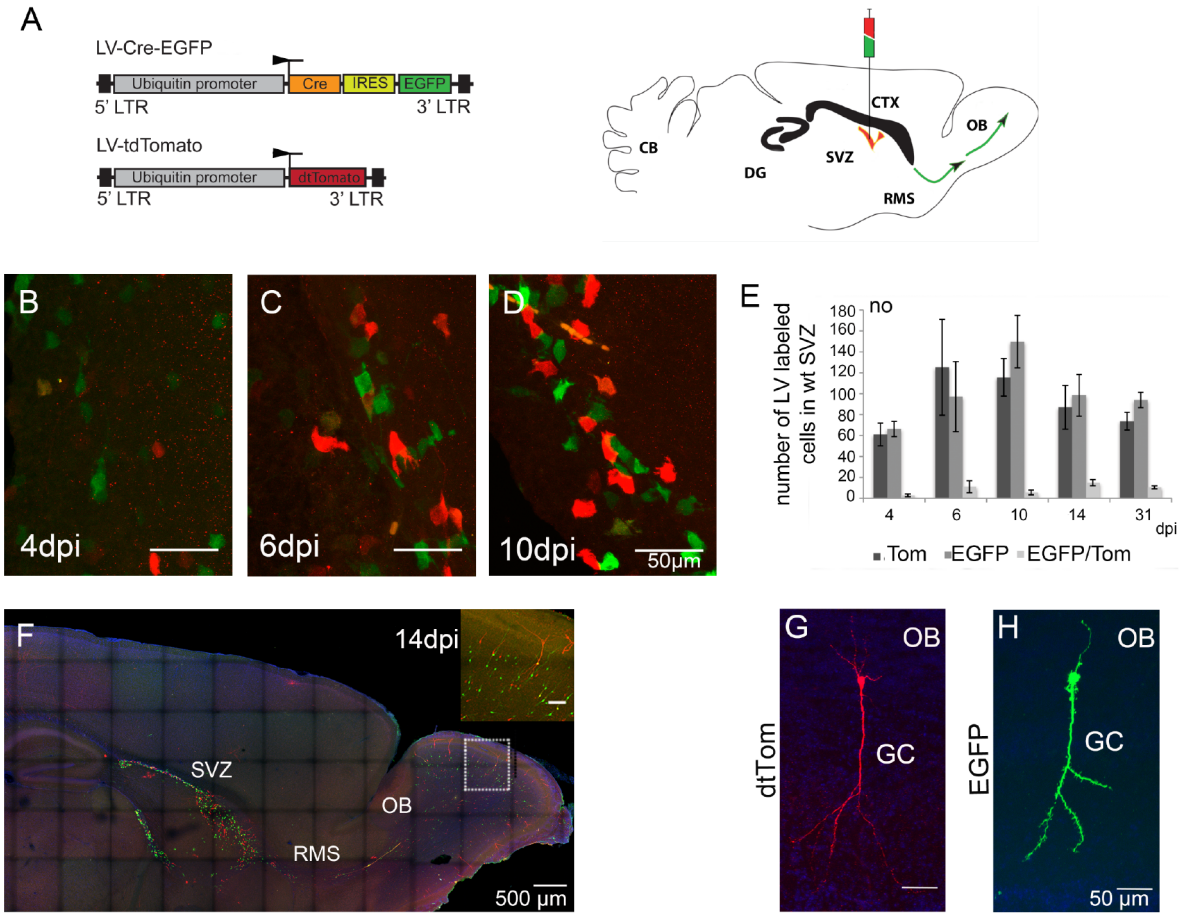

Figure 2 | LV delivery into the SVZ of postnatal wt mice. (A) A schematic drawing showing the lentiviral vectors used for injection (left). LV-Cre-EGFP induces the γ-pcdh conditional ko and labels cells with EGFP (green), LV-tdTom infects wt cells, labled in red. Schematic drawing of an adult mouse brain showing the injection site in the SVZ, the syringe demonstrating the 'cocktail injection' of the LV-Cre-EGFP (in green) and LV-tdTom in red (right). The SVZ is marked in red color, green arrows indicate the RMS. (B–D) Cell morphology of LV infected cells ($EGFP^+$ cells in green; Tom^+ cells in red) in the SVZ at 4, 6, and 10 dpi. (E) Bar-graph showing the numbers of Tom^+, $EGFP^+$ and Tom^+, $EGFP^+$ double positive cells in the SVZ at 4, 6, 10, 14 and 31 dpi, indicating a stable infection efficacy by both LVs (ANOVA, $p < 0.001$; Student's t-test, $p < 0.05$). (F) A parasagittal section of a wt brain at 14 dpi showing distribution of $EGFP^+$ (green, γ-pcdh deficient) and Tom^+ (red, wt) cells in the SVZ, the RMS, and in the OB. Close-up showing infected olfactory granule cells. (G, H) Tom^+ and $EGFP^+$ labeled olfactory GCs in a parasagittal section at 21 dpi showing similar signal intensity and morphology after LV infection. Scale bars in B–D 50 µm, in F 500 µm, in inset 100 µm, in G, H 50 µm.

individual LVs in SVZ progenitor cells we divided the number of Tom^+ cells by the number of $EGFP^+$ cells and calculated the ratio at two different stages after virus application (Table 1, n = 3 mice, 3 sections/mouse). These ratios suggest constant infection efficacies of the two different LVs suggesting that virus-mediated Cre expression does not affect cell survival.

To accomplish comparable fluorophore intensities for a morphological comparison of cells, we enhanced EGFP and tdTomato in all experiments by immunolabeling (Fig. 2B–D, F, and Methods). Concomitantly we found bright Tom^+ and $EGFP^+$ GCs in the OB at 21 dpi (Fig. 2G, H), allowing comparative morphological analysis.

Ablation of γ-pcdhs in SVZ progenitor cells of γ-$pcdh^{lox/lox}$ mice. We next ablated γ-pcdhs in the SVZ of γ-$pcdh^{lox/lox}$ mice by LV-mediated Cre expression. As in the experiments described above, in γ-$pcdh^{lox/lox}$ mice, LV mediated expression of EGFP selectively marked Cre positive γ-pcdh ko cells, whereas LV driven expression of tdTom visualized "unfloxed" wt cells. This approach allowed a

Table 1 | Quantitative evaluation [%± SEM] for $EGFP^+$ and Tom^+ cells in postnatal injected wt and γ-$pcdh^{lox/lox}$ mice

wt	SVZ	SVZ	SVZ	OB	OB	OB/SVZ	OB/SVZ
Age [dpi]	Tom^+	$EGFP^+$	$Tom^+/EGFP^+$	Tom^+	$EGFP^+$	Tom^+	$EGFP^+$
14	46.9 ± 1.2	53.1 ± 1.2	0.9	58.4 ± 2.1	41.6 ± 2.6	2.1	1.4
31	43.9 ± 1.1	56.0 ± 0.9	0.8	85.5 ± 1.3	14.5 ± 2.2	4.8	1.2
γ-$pcdh^{lox/lox}$	SVZ	SVZ	SVZ	OB	OB	OB/SVZ	OB/SVZ
14	19.2 ± 1.2	80.7 ± 0.8	0.3	33.2 ± 4.0	66.7 ± 1.0	1.7	0.8
21	15.4 ± 1.3	63.0 ± 1.0	0.3	53.8 ± 1.2	46.1 ± 1.6	3.5	0.5
42	27.3 ± 1.3	84.5 ± 2.0	0.4	46.6 ± 1.5	53.4 ± 2.7	1.7	0.7

direct side-by-side comparison of γ-pcdh ko cells with "unfloxed" wt cells during postnatal development. A first visual inspection of cellular morphology revealed no differences between $EGFP^+$ and Tom^+ cells in SVZ at 4, 6 and 10 dpi (Fig. 3A–C, Table S1) and at 14, 21, and 42 dpi (Table S1). Additional cell counting of $EGFP^+$ and Tom^+ cells in the SVZ at these time points showed no significant differences in cell numbers or in the ratios of Tom^+ to $EGFP^+$ cells over the time points analyzed (Table 1, Fig. 3D, Student's t-test, ANOVA, n = 3 mice per stage, 3–6 brain sections per mouse), indicating stable populations of virus-infected cells over time.

To demonstrate γ-pcdh loss in $EGFP^+$ cells in the SVZ we performed immunolabeling for EGFP and γ-pcdh expression in γ-$pcdh^{lox/lox}$ and wt mice at 4, 6, 10, and 14 dpi after LV cocktail injections at P0 (shown for γ-$pcdh^{lox/lox}$ at 6, 10 and 14 dpi, Fig. 3E–G). In γ-$pcdh^{lox/lox}$ mice cell counting for EGFP and γ-pcdh positive cells revealed an increase in $EGFP^+$ (γ-$pcdh^-$) cells in SVZ progenitors from 7.4 ± 3.7% at 4 dpi to 76.6 ± 14.0% at 14 dpi (Fig. 3H, Student's t-test, $p < 0.05$, n = 2 mice). At 14 dpi we also counted a small percentage of $EGFP^+$/γ-$pcdh^+$ double positive cells (9.0 ± 4.2%, n = 2 mice). From these results we conclude that LV-Cre-EGFP specifically ablated functional γ-pcdh expression in infected cells in the SVZ starting from 4 dpi. The EGFP/γ-pcdh double labeling at 14 dpi may indicate an incomplete and premature state of some γ-pcdh ko progenitor cells.

To identify the type of neural progenitors that can be infected in the SVZ, we performed LV-Cre-EGFP injections into the SVZ of neonatal $pcdh^{lox/lox}$ mice and assessed their identity at 14 dpi. Immunolabeling for neural markers of the SVZ at 14 dpi showed that LV-Cre-EGFP infected B-type stem cells, C-type transit amplifying cells and A-type neuroblast[25–27] as shown by co-expression of EGFP/GFAP indicating LV infection of B-type stem cells (Fig. 3I), and EGFP/Sox2 (Fig. 3K), indicating LV infection of C-type transit amplifying cells. We further showed co-expression for EGFP/Dcx indicating LV infection of A-type neuroblasts (Fig. 3L). We surmise

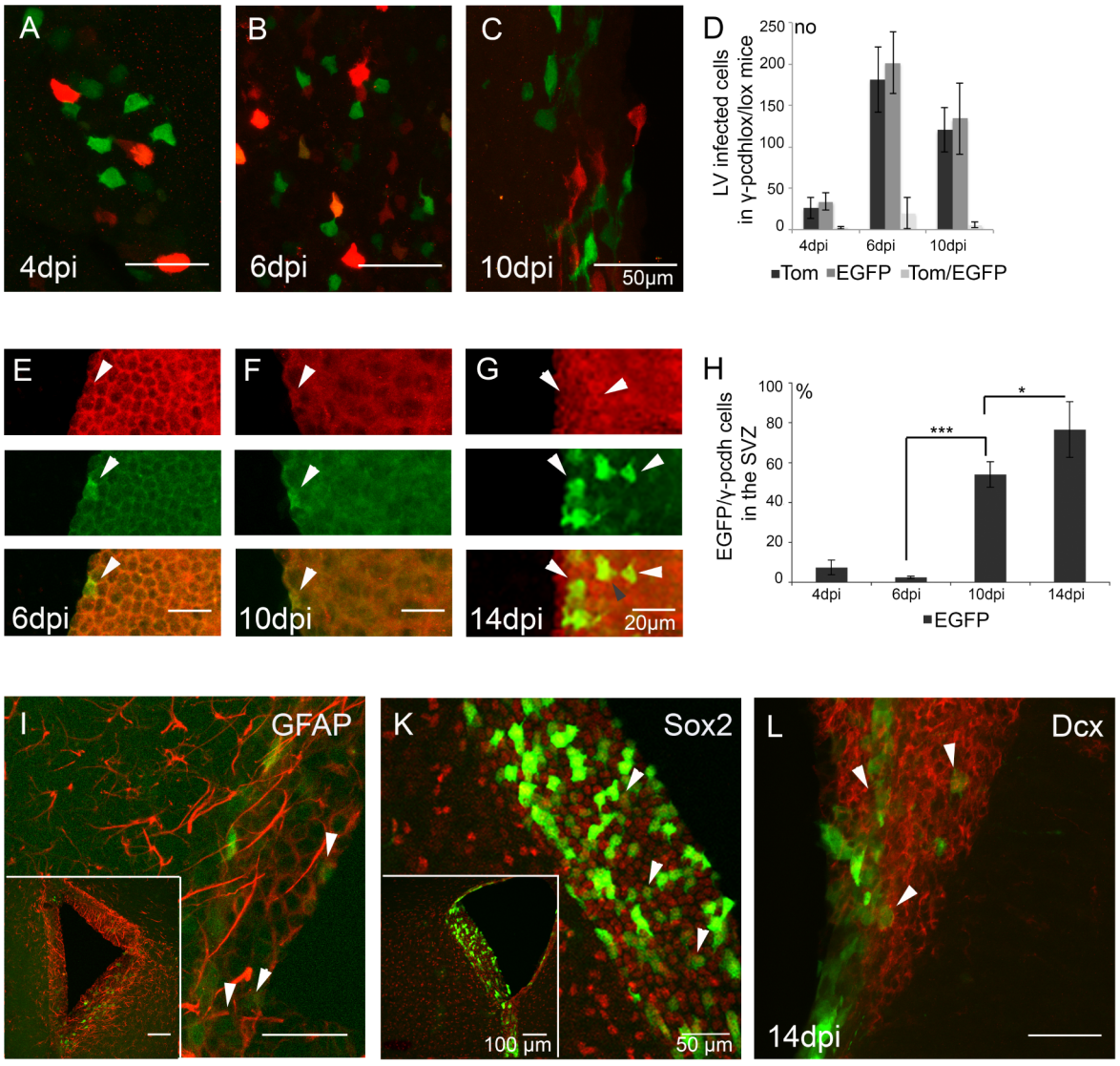

Figure 3 | $EGFP^+$ γ-pcdh deficient cells in the SVZ. (A–C) Morphological comparison of $EGFP^+$ and Tom^+ cells in the SVZ of γ-$pcdh^{lox/lox}$ injected mice at 4, 6, and 10 dpi. (D) Quantitative analysis of $EGFP^+$, Tom^+ and $EGFP^+/Tom^+$ double-positive cells in the SVZ at 4, 6, and 10 dpi. (E–G) Immunolabeling for EGFP and γ-pcdh expression in γ-$pcdh^{lox/lox}$ injected mice at 6, 10, and 14 dpi, showing of $EGFP^+$/γ-$pcdh^-$ (green, white arrows), γ-$pcdh^+$ (red, white arrows) and $EGFP^+$/γ-$pcdh^+$ (yellow, grey arrow) expression in single and merged layers. (H) Quantitative analysis of the percentage of $EGFP^+$ cells in the SVZ at 4, 6, 10 and 14 dpi. (I–L) Immunolabeling for neural stem cell markers on parasagittal sections at 14 dpi showing co-expression of EGFP with GFAP (I, white arrows, inset SVZ), Sox2 (K, white arrows, inset SVZ), and Dcx (L, white arrows, inset SVZ). Scale bars in A–C, 50 µm, in E–G, 20 µm, in I–L 50 µm, in insets 100 µm.

that LV-Cre-EGFP infected B-, C-, and A-type SVZ progenitor cells. Furthermore we showed that LV-Cre-EGFP ablated functional γ-pcdh expression in infected SVZ cells starting from 4 dpi.

Proliferation properties of EGFP$^+$ γ-pcdh ko cells. To see whether EGFP$^+$ γ-pcdh ko cells show aberrant differentiation we screened for morphological differences in γ-pcdh$^{lox/lox}$ injected mice in the OB at 14, 21, and 42 dpi, according to the regular morphological development of dendrites and synapses in olfactory GCs[18,28]. A first visual inspection already suggested differences in cell numbers and morphology of EGFP γ-pcdh ko, compared to Tom$^+$ wt cells in the OB at 14, 21, and 42 dpi (Fig. 4A–C). While Tom$^+$ neurons displayed regular GC development, EGFP$^+$ neurons developed abnormally (Fig. 4A–C). We quantified differences in cell numbers and evaluated the migration rate of EGFP$^+$ and Tom$^+$ neurons. To this end EGFP$^+$ and Tom$^+$ cells were counted in the OB and in the SVZ at 14, 21, and 42 dpi (n = 3 mice, 3–6 brain sections per mouse, Fig. 4D). Subsequently we divided the number of EGFP$^+$ cells in the OB by the number of EGFP$^+$ cells in the SVZ and did the same calculation for Tom$^+$ cells. The results revealed a decrease in the number of EGFP$^+$ neurons that reached the OB at all three stages analyzed when compared to Tom$^+$ cells (Fig. 4D; Table 1; Student's t-test, $p < 0.05$). Note that the ratio of EGFP$^+$ cells in the OB compared to the SVZ and the ratio of Tom$^+$ cells in the OB compared to the SVZ of wt injected mice at 14 and 31 dpi showed a similar tendency (Table 1), although the ratio of EGFP$^+$ cells was reduced compared to Tom$^+$ cells. These results suggest a reduced number of EGPF$^+$ compared to Tom$^+$ neurons that reached the OB. As a control for the morphological defects found in EGFP$^+$ olfactory GCs in γ-pcdh$^{lox/lox}$ injected mice, we next compared EGFP$^+$ and Tom$^+$ olfactory GCs in wt injected mice at 10 and 14 dpi by Sholl analysis. The results showed a similar morphology of EGFP$^+$ and Tom$^+$ neurons in dendritic branching and in the length of the apical dendrites (Fig. 4E–I, Table S3, Student's t-test, n = 3 mice, 12 GCs per stage and LV), confirming the phenotypic alterations found in EGFP$^+$ olfactory GCs in LV injected γ-pcdh$^{lox/lox}$ mice.

Despite the differences in cell numbers of EGFP$^+$ and Tom$^+$ infected cells, immunolabeling for Dcx and NeuN showed

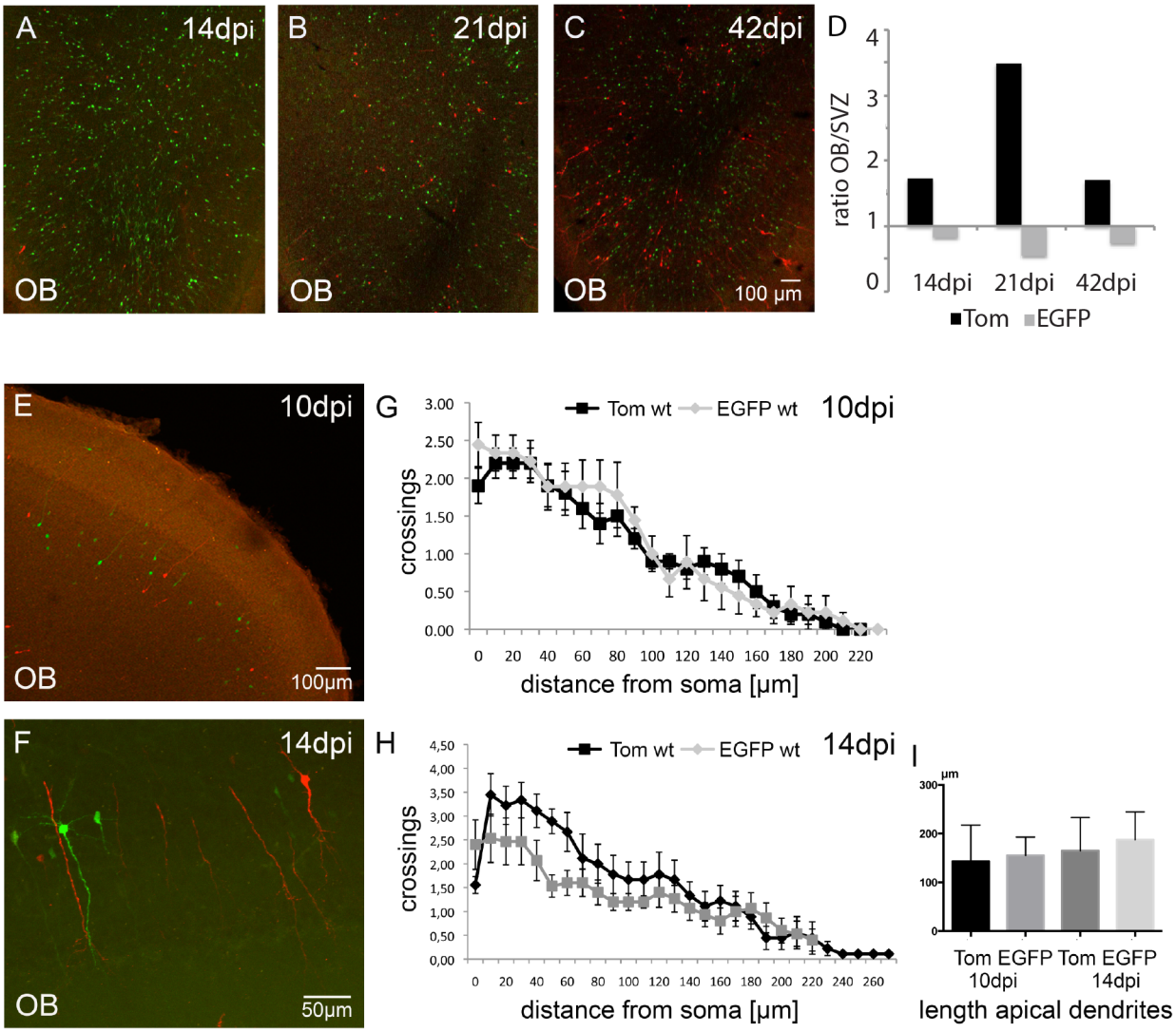

Figure 4 | Neurogenesis of EGFP$^+$ γ-pcdh ko cells. (A–C) Immunolabeling for EGFP and tdTom in γ-pcdh$^{lox/lox}$ injected mice showing EGFP$^+$ and Tom$^+$ olfactory GCs in the OB at 14, 21, and 42 dpi. (D) Bar-graph showing a higher ratio (OB/SVZ) in Tom$^+$ cells compared to EGFP$^+$ cells, indicating less EGFP$^+$ than Tom$^+$ cells that reach the OB. (E, F) Immunolabeling for EGFP$^+$ and Tom$^+$ cells in wt injected mice at 10 and 14 dpi, showing similar fluorophore intensities. (G, H) Sholl analysis for EGFP$^+$ (grey) and Tom$^+$ (black) olfactory wt GCs at 10 and 14 dpi showing no significant differences in dendritic branching. (I) Bar-graph showing quantitative analysis for apical dendrite length for EGFP$^+$ (grey) and Tom$^+$ (black) olfactory wt GCs at 10 and 14 dpi. Scale bars in C 100 µm, representable for A and B, in E 100 µm, in F 50 µm.

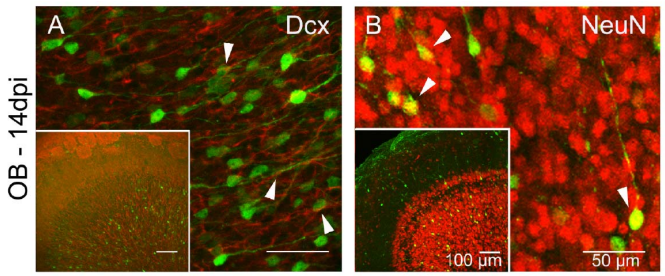

Figure 5 | LV infected EGFP$^+$ cells in the OB express neuronal markers. (A) Immunolabeling showing co-expression of EGFP (green) and Dcx (red, white arrows) and in olfactory GCs on a parasagittal section at 14 dpi. Inset showing overview of OB. (B) Immunolabeling showing co-expression of EGFP (green) and NeuN (red, white arrows) on a parasagittal section at 14 dpi. Inset showing an overview of the OB. Scale bars in A, B 50 µm, in insets 100 µm.

co-expression of EGFP/Dcx and EGFP/NeuN in the OB demonstrating their neuronal identity (Fig. 5A, B). Therefore we suggest that the EGFP$^+$ cells that reached the OB at 14 dpi acquired neuronal identity.

To test whether the differences in number of EGFP$^+$ versus Tom$^+$ neurons in the OB were due to aberrant proliferation of EGFP infected progenitor cells in the SVZ, we next analyzed the proliferation rate of EGFP$^+$ and Tom$^+$ cells in the SVZ. Proliferating stem cells in the SVZ can be labeled with 5-bromo-2′-deoxyuridine (BrdU), and their migration into the cortex and the OB can subsequently be followed[29,30]. To quantify newly generated EGFP$^+$ and Tom$^+$ cells in the SVZ we injected intraperitoneal 5-bromo-2′-deoxyuridine (BrdU, 20 mg/KG) 4 days after LV application into the SVZ of perinatal γ-pcdh$^{lox/lox}$ and wt mice (see Methods). EGFP$^+$/BrdU$^+$ double positive cells were analyzed in the SVZ two hours, two- and six days after BrdU injection (according to 4, 6, and 10 dpi; shown for 6 and 10 dpi, Fig. 6A, B). In general, two hours after the last BrdU injection at 4 dpi, the percentage of doubled labeled cells was low (Fig. 6C). We found slightly increased numbers of BrdU$^+$/EGFP$^+$ cells at 6 dpi and 10 dpi compared to BrdU$^+$/Tom$^+$. However statistical analysis of double-positive cells (BrdU$^+$/EGFP$^+$ and BrdU$^+$/Tom$^+$) in γ-pcdh$^{lox/lox}$ mice at all three time-points showed no significant differences in proliferation between EGFP$^+$ and Tom$^+$ infected cells (Student's t-test, n = 3 mice per stage, 3–6 sections per mouse, Fig. 6C, Table S2). An additional analysis of proliferating progenitor cells in wt injected mice at 4, 6, and 10 dpi did not reveal significant differences in the percentage of EGFP$^+$ and Tom$^+$ cells (Table S2, Student's t-test, n = 3 mice per stage, 3–6 sections per mouse). From these results we conclude that newly generated EGFP$^+$ γ-pcdh ko cells proliferated regularly in the SVZ.

Morphology of EGFP$^+$ γ-pcdh ko olfactory GCs. Since published work suggested a functional link between the loss of γ-pcdhs and defects in dendritic architecture in cortical neurons[10], we investigated whether EGFP$^+$ γ-pcdh deficient neurons show morphological alterations in olfactory GCs.

Although EGFP$^+$ γ-pcdh deficient and neurons show neuronal characteristics as shown by NeuN and Dcx co-immunolabeling (Fig. 5A, B), closer inspection, as mentioned above, suggested that dendrite morphology of EGFP$^+$ γ-pcdh ko olfactory GCs was affected (Fig. 7A–F, see also Fig. 4A–C). Thorough quantification of the length of apical dendrites and arbor complexity in EGFP$^+$ neurons by Sholl analysis at 14, 21, and 42 dpi (Fig. 7G–I, n = 3 to 5 mice per stage; 15 section per mouse, see Methods) revealed a decrease in apical dendrite length and reduced arbor complexity in EGFP$^+$ γ-pcdh ko GCs compared to Tom$^+$ wt neurons starting from 14 dpi (Fig. 7K, L). At 14 dpi, dendritic branching in EGFP$^+$ GCs was significantly reduced compared to Tom$^+$ GCs (Fig. 7G, L, Table S3, Student's t-test, $p < 0.05$). Yet, no significant reduction was found in the length of apical dendrites in EGFP$^+$ neurons (Fig. 7G, K, Table S3, Student's t-test). At 21 dpi EGFP$^+$ neurons displayed similar characteristics compared to 14 dpi (Fig. 7H, Table S3, Student's t-test, $p < 0.05$). The apical dendrites of EGFP$^+$ neurons were not significantly reduced in length when compared to Tom$^+$ GCs at 21 dpi (Fig. 7K, Table S3, Student's t-test), whereas at 42 dpi EGFP$^+$ neurons exhibited a severe reduction in both, arborization and length of apical dendrites compared to earlier stages analyzed (Fig. 7I–L, Table S3, Student's t-test, $p < 0.001$).

We next asked whether the morphological changes in γ-pcdh deficient GCs have consequences for synapse formation. In adult olfactory GCs new synapses form in a dynamic pattern in the apical part of the dendrites and form dendro-dendritic synapses in the distal part[17]. To see whether loss of γ-pcdhs affects dendritic spine formation in olfactory GCs, we counted the number of dendritic spines in Tom$^+$ wt and EGFP$^+$ γ-pcdh deficient GCs at 14 and 21 dpi (n = 5 mice, 15 neurons per genotype and stage). The result revealed a significant reduction in spine number in EGFP$^+$ neurons at 14 dpi when compared to the number of spines in Tom$^+$ neurons. Accordingly, a significant reduction of spine number was detected in EGFP$^+$ neurons at 21 dpi compared to Tom$^+$ GCs (Fig. 7M; Table S3, Student's t-test, 14 dpi: $p < 0.0001$, 21 dpi: $p < 0.05$). At 42 dpi, no spines could be detected anymore in EGFP$^+$ γ-pcdh ko neurons.

These results suggest that loss of functional γ-pcdh expression leads to reduced dendrite complexity and spine formation starting from 14 dpi onwards with a gradual increase in these defects. We conclude that regular olfactory GC development demands functional γ-pcdh expression.

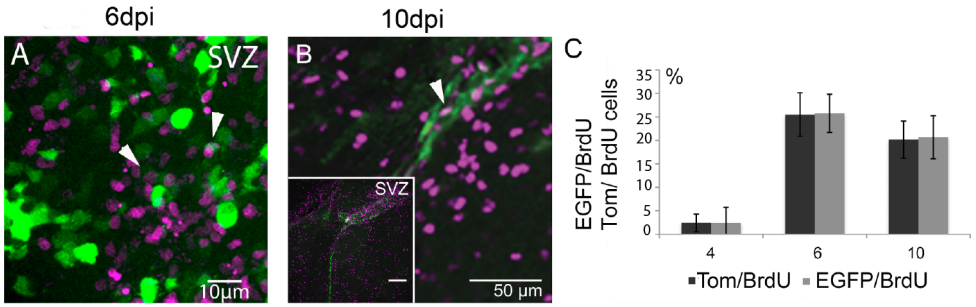

Figure 6 | Proliferation of LV-infected EGFP$^+$ and Tom$^+$ cells. (A, B) Immunolabeling of EGFP$^+$/BrdU$^+$ positive cells on a parasagittal sections from mouse brains at 6 and 10 dpi, showing the distribution of fluorescently labeled cells and co-expression of BrdU and EGFP in the SVZ (white arrows). (C) Bar-graph showing a quantitative analysis of Tom$^+$/BrdU$^+$ and EGFP$^+$/BrdU$^+$ cell numbers in the SVZ in [%]. Scale bars in A 10 µm, in B 50 µm, in inset 100 µm.

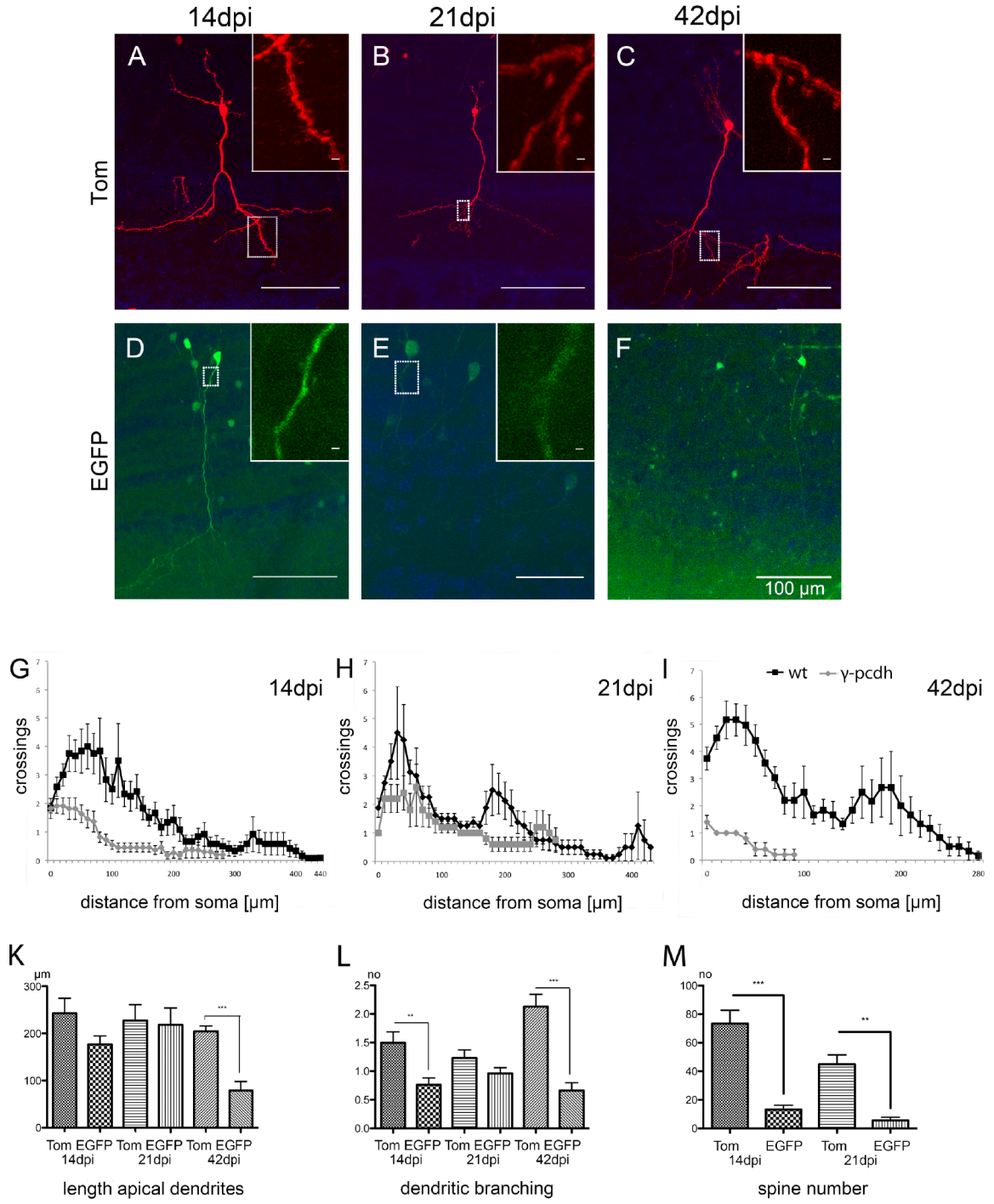

Figure 7 | Morphology of LV-infected EGFP$^+$ and Tom$^+$ olfactory GCs. (A–F) Morphology of olfactory EGFP$^+$ and Tom$^+$ GCs analyzed at 14, 21, and 42 dpi. (A, D) A parasagittal section from γ-pcdh$^{lox/lox}$ injected mice showing a reduction in dendritic arborization of EGFP$^+$ cells at 14 dpi. Insets showing magnification with spines on Tom$^+$ (A) and on EGFP$^+$ (D) dendrites at 14 dpi. (B, E) Parasagittal section at 21 dpi showing a reduction of dendritic arborization in EGFP$^+$ cells (E). Insets showing magnification of dendrites on Tom$^+$ (with spines B) and of EGFP$^+$ (E) dendrites at 21 dpi. (C, F) Parasagittal section at 42 dpi showing prominent dendrites and spines only in Tom$^+$ GCs (C). Note that EGFP$^+$ GCs (F) have shorter dendrites and lack spines. (G–I) Sholl analysis for dendrite morphology of EGFP$^+$ and Tom$^+$ olfactory GCs at 14, 21, and 42 dpi (wt in black, γ-pcdh ko cells in grey). (K–L) Bar-graphs showing quantitative analysis for length of apical dendrites (K), dendritic branching (L), and spine numbers (M). Scale bars in A–F 100 µm, in insets 10 µm.

Discussion

Identification of genes involved in the differentiation of olfactory GCs is crucial for an interpretation of the functioning of neuronal networks in the adult olfactory bulb. As shown recently, γ-pcdhs are important for synaptic development and connectivity in retinal ganglion cells, interneurons of the spinal cord and cortical neurons[8,10,19]. Here we provide first evidence that functional ablation of γ-pcdhs in SVZ progenitor cells results in aberrant dendrite and spine development of newborn olfactory GCs.

Lentiviruses are frequently used for the induction of conditional kos in defined cell populations of mice[31,32], including the ablation of genes in SVZ progenitors[33,34]. The expression of the desired gene in

specific progenitor populations[35] allows a selective investigation during neuronal differentiation and maturation processes. In this study the use of LV-mediated Cre recombinase expression in a conditional γ-pcdh ko mouse line resulted in the ablation of γ-pcdhs in B-, C-, and A-type SVZ progenitors[11], as shown with immunolabeling for GFAP, Sox2, and Dcx, marker genes for B-, C-, and A-type SVZ progenitors. Our results suggest that LV infection of B-type and C-type progenitors results in a complete loss of γ-pcdh expression after successive rounds of self-renewal[36], which finally results in migrating progenitor populations completely lacking functional γ-pcdh expression. However, as those types of neuronal stem cells divide with different proliferation rates[37], we suggest that LV-mediated γ-pcdh ablation leads to a heterogeneous population of infected cells, which in turn results in a mixed population of differentiated GCs in the OB. Nevertheless, since our experiments showed that BrdU incorporation revealed no difference in proliferation rates of γ-pcdh ko cells when compared to wt cells as early as 4 dpi, we surmise that ablation of γ-pcdhs is not biased towards select stem cell types and additionally does not alter proliferation rates in early progenitors. Thus, a heterogenous pool of γ-pcdh ablated progenitor cells in the SVZ likely leads to heterogenous populations of γ-pcdh deleted GCs in the OB. With respect to this heterogenous pool of olfactory GCs the time point of γ-pcdh ablation after stereotaxic injection is crucial. In our experiments, γ-pcdh ablation in γ-pcdh$^{lox/lox}$ mice was observed by immunolabeling as early as 4 dpi. As the onset of β-galactosidase expression after LV-Cre-EGFP injection into Rosa26 reporter mice occurs ~24 hrs after stereotaxic virus delivery, we suggests that the γ-pcdh alleles are floxed in γ-pcdh$^{lox/lox}$ mice between 24 and 48 hrs. Note that a pool of γ-pcdhs, which was already expressed before Cre-mediated gene deletion, likely remains stable for prolonged periods of time. However, as we assume that Cre expression starts as early as ~24 hours after stereotaxic delivery, these early arriving progenitor cells are fastly exchanged by subsequently arriving γ-pcdh deficient progenitor cells in the OB.

The γ-pcdh deficient precursors that reach the OB showed morphological defects with respect to dendrite length and dendritic arborization. One possibility for these defects might be an arrest of olfactory GC differentiation due to the loss of γ-pcdhs. Migrating wt progenitors successively develop complex dendritic arbors and spines after reaching the OB and can be categorized in the fully differentiated state as class 5 olfactory neurons[15]. Tom$^+$ wt GCs and EGFP$^+$ GCs in wt control injections show prominent dendritic branching and spines and therefore likely represent class 5 olfactory GCs. The fact that the vast majority of EGFP$^+$ γ-pcdh ko GCs lack complex dendrites and spines from 14 dpi onwards indicates that these neurons cannot progress their development into class 5 olfactory GCs. Alternatively, the loss of γ-pcdhs in olfactory GCs may lead to an early onset of neuronal death. The reduced cell numbers of EGFP$^+$ cells in the OB starting from 14 to 42 dpi might suggest this possibility. Whether the γ-pcdh ko GCs apoptose, or do not properly develop cannot be concluded from our observations, however, accordingly, apoptosis appears to be enhanced in γ-pcdh ko retinal ganglion cells[8] and spinal cord interneurons[9]. Since we cannot exactly quantify the amount of remaining γ-pcdhs in olfactory CGs, we estimated the onset of γ-pcdh gene deletion and the time point when all cells that reached the OB showed morphological deficits. Accordingly, at ~42 dpi all EGFP$^+$ GCs in the OB showed severe deficits in dendrite- and spine formation, suggesting that these cells lack γ-pcdhs, or alternatively that the remaining γ-pcdh pool in these cells is insufficient for proper GC development. Interestingly, in cortical projection neurons of Layer V, γ-pcdh loss also resulted in reduced dendrite arborization[10], however synaptic density appeared unaffected. In contrast, Wang and colleagues[19] suggested that the death of γ-pcdh deficient spinal cord interneurons was due to a lack of functional synapses. A recent study of Lefebvre and colleagues showed that γ-pcdhs display interrupted self-avoidance of dendrites in retinal starburst amacrine cells and in cerebellar Purkinje cells[38]. We here show a critical function for γ-pcdhs in dendritic and spine development of adult-born GCs in the OB.

Methods

Ethic statement. All animal experiments were conducted under the license 35-915.81/G171/10 at the regional council in Karlsruhe and are in accordance with the guidelines of the Max Planck Society.

Mice. We used C57BL/6 male and female wild type (wt) mice (Charles River, Sulzfeld, Germany) and conditional 'floxed' γ-pcdh$^{lox/lox}$ or complete γ-pcdh ko mice[5] backcrossed for 6 generations into a C57BL/6 background. The day of birth was determined as P0. All mice were maintained under standard conditions, 12 hrs dark/light cycles with water and food ad libitum.

Lentivirus production. Lentiviruses were produced as previously described[39], with small modifications[40]. Briefly, human embryonic kidney 293FT cells (Invitrogen; Carlsbad, CA) were transfected by using the calcium-phosphate method with three plasmids: expression vector and two helper, 8.9 and vesicular stomatitis virus G protein vectors at 1, 7.5, and 5.5 μg of DNA per 10-cm plate. After 48 hrs, the supernatants of 10 plates were pooled, spun at 780 g for 5 min, filtered with a pore size 0.45 μm, spun at 83.000 g for 1.5 hrs, and the pellet was finally resuspended in 100 μl of PBS (pH 7.4). EGFP linked with an internal ribosomal entry site to Cre, as well as tdTomato were expressed from a lentiviral expression vector under the control of the ubiquitin core promotor[41]. Prior to stereotaxic injections all viruses were tested for functionality and tittered in rat primary cortical neurons with serial dilutions of purified virus solution (1, 1 : 10, 1 : 100, 1 : 1000; number of fluorescent neurons x dilution factor = infectious particles/μl). The LV we used here for injections all contained ~10^4 infectious particles/μl.

Stereotaxic virus injections. Young adult C57BL/6 mice (P28, P42) were anaesthetized with a mixture of ketamine and xylazine (100 mg/kg and 10 mg/kg, respectively) injected intraperitoneally. Mice were head-fixed using non-puncture ear bars and a nose clamp (David Kopf Instruments, Tujunga, California, USA), and their body-temperature was maintained at 36–37°C using a heating blanket (FHC, Bowdoin, Maine, USA). An incision was made in the scalp and a small craniotomy was drilled above the relevant area of the brain using a dental drill (Foredom Electric, Bethel, Connecticut, USA). Subsequently, the dura was removed. The surface of the brain was kept moist by applying sterile PBS (Sigma Aldrich, St. Louis, Missouri, USA) at regular intervals. For injections, glass pipettes were pulled with a tip size of approximately ~4 μm diameter and tip-filled using negative pressure. Injection pipettes were lowered as accurately as possible. Coordinates for stereotaxic injections into the SVZ were: Bregma: 0.5 mm, Lateral: 0.75 mm, Ventral: 1, 7 mm. Approximately, 2 μl of LV-containing solution was injected under constant positive pressure for ~30 minutes. Following stereotaxic injection the scalp was sutured. The time from the initial anesthesia to completing this procedure was kept as short as possible (~1 hour). During recovery, mice were kept warm on a heating plate (37°C) for 6 hrs.

LV injections into SVZ of newborn mice (P0) were performed as described in Pilpel and colleagues[41]. Briefly, pubs were removed from their mother and anaesthetized on ice for 5 min. 2 μl of LV containing solution was injected into both ventricles using a 34-gauge needle and a microprocessor infusion pump (injection speed: 125 nl/s). After injection, mice were put on a warming plate (37°C) to recover and put back to their mother after recovery[41].

Generation of floxed γ-pcdh allele and genotyping. We previously reported the generation of different lethal γ-pcdh ko mouse lines[5]. As homozygous mice, carrying the *pgk-neo* cassette are not viable for more than 3 hours after birth, we here generated a viable floxed γ-*C1* mouse line allowing for conditional, Cre-mediated γ-pcdh deletion in adult mice. We therefore removed the expression-attenuating, lethal *pgk-neo* cassette from the floxed "neo allele" by crossing our γ-pcdh '3Lox'- mice[5] with EIIaCre mice (see Figure 1A). The crossings resulted in ubiquitous partial *in vivo* Cre-recombinations with subsequent allelic segregation in the next generation. Biallelic excision of *pgk-neo*, routinely checked by PCR, resulted in a reversion of the lethal phenotype and a mouse line, γ-pcdh$^{lox/lox}$, in which γ-*C1* was solely flanked by two *LoxP* sites.

Immunohistochemistry. For immunohistochemical analysis, mice were killed at 4, 6, 10, 14, 21, and 42 days after injection. Mice were deeply anaesthetized with isofluran (Baxter Inc.) and transcardially perfused with 0.1 × PBS for 3 min followed by 4% PFA in 0.1 M phosphate buffer (PB, pH 7.2) for 7 min. Brains were carefully removed from surrounding tissue and post-fixed in 4% PFA over night at 4°C. Brains were embedded in 3% agarose and sectioned (70–100 μm) with a vibratome (Leica VT1000, Leica Microsystems, Germany). Selected sections were incubated for 1 hr in blocking solution (5% normal goat serum (NGS), 1% Triton X-100, in PBS) followed by overnight incubation in primary antibody: BrDU (5-bromo-2′-deoxyuridine, Accurate Chemical & Scientific Corporation), 1 : 250; Doublecortin (abcam), 1 : 1000; dsRED (Clontech), 1 : 1000; GFP (abcam), 1 : 5000; GFAP (DakoCytomation), 1 : 1000; NeuN (abcam), 1 : 800; Sox2 (abcam), 1 : 500; and γ-pcdh, 1 : 1000[5]. After 12 hrs sections were washed 3 times 10 min in PBS and incubated for 2 hrs with secondary antibodies (anti-rabbit/mouse Cy-3 conjugated, Jackson Laboratories,

1 : 300, or Alexa-fluor 488 conjugated, Invitrogen, 1 : 400, in 1% NGS, 0.5% Triton X-100 in PBS), followed by 3 washes in PBS. To remove residual salt, sections were washed for 2 min in 10 mM Tris/HCl and mounted on Superfrost plus slides (Thermo scientific), dried for 10 min, and covered with glycerol (80% glycerol, 0.5% w/w DABCO (1,4-Diazabicyclo[2.2.2]octane, 1.4500 nD at 20.1°C in PBS, pH 8.9, Sigma D2522).

X-Gal staining. 100 μm vibratome sections were incubated in X-Gal staining buffer (5 mM K4Fe(CN)6, 5 mM K3Fe(CN)6, 2 mM MgCl2, 2 mg/ml X-Gal) for ~5 hrs at 37°C, washed 3 times for 10 min in PBS (pH 7.4), and incubated ~2 min in 10 mM Tris/HCl pH 7.4 before mounting on Superfrost plus slides (Thermo scientific) with Aqua Polymount (Polysciences).

Nissl staining. 100 μm vibratome sections were mounted on Superfrost plus slides (Thermo scientific) and incubated for ~40 sec in Nissl solution (0.1% Thionin in H_2O, Sigma), washed 3 times in water and dehydrated stepwise (5 min each; 70%, 95% and 100% in water), followed by a final wash in Xylol. Slides were mounted with Eukitt-quick-hardening mounting medium (Fluka).

Birthdating analysis with BrdU. 20 mg/kg Bromodeoxyuridine (5-bromo-2′-deoxyuridine, BrdU; Accurate Chemical & Scientific Corporation) was injected intraperitoneally in perinatals 4 days after LV delivery (five injections spaced by 2 hrs). For analysis mice were killed 4 hrs, two and six days after BrdU application. To quantify the amount of BrdU/EGFP and BrdU/Tom double-positive cells, 3–6 parasagittal sections of 3 mice at each stage were imaged with a Leica confocal microscope (Leica TCS SP5, Leica Microsystems). Double-positive cells were counted using the cell counter plugin of Fiji (ImageJ). Statistical analysis was performed using the program Prism. Student's t-test was applied to compare γ-pcdh ko versus wt cells. Values are expressed as mean ± SEM.

Morphological analysis of olfactory granule cells. Sholl analysis was performed to quantify the complexity of dendritic arborization of individual neurons. Dendritic arborization was measured in confocal reconstruction of whole neurons with crossing measured in concentric circles of 10 μm increments from the soma. Confocal images were analyzed using the plug-in 'Simple Neurite Tracer and 'Sholl analysis' from Fiji (ImageJ). 15 neurons from each stage were analyzed. Statistical analysis was performed using Prism. An unpaired Student's t-test was applied to compare wt versus γ-pcdh ko olfactory granule neurons. Values are expressed as mean ± SEM.

The length of apical dendrites was calculated from data obtained from the analysis for dendritic arborization by the Fiji plug-in 'Simple Neurite Tracer'. Spine numbers were obtained from individual $EGFP^+$ and Tom^+ olfactory granule neurons at 14 and 21 days after injection (n = 15 neurons per stage, 3 mice). Spines were counted in distal, apical and proximal dendritic areas from maximal projections of confocal image z-stacks of 70 μm thickness. The average branching was defined as the total number of branches from all neurons analyzed. Statistical analysis was performed using the program Prism. Unpaired Student's t-tests were applied to compare wt with γ-pcdh ko olfactory granule neurons. Values are expressed as mean ± SEM.

Western blot. For Western blot (WB) analysis mouse brains were solubilized in 25 mM HEPES, [pH 7.5], 150 mM NaCl, protease inhibitor cocktail (Roche), containing 1% Triton X-100 (TX-100). SDS-PAGE and blotting were performed using standard conditions. γ -ICD rabbit polyclonal antiserum[5] was diluted 1 : 500. For visualization blots were developed with a table processor (Optimax Type TR, Protec, Germany). Quantification of WBs was performed with ImageJ-software.

Microscopy and statistical analysis. All images were taken with a laser scanning confocal microscope (Leica TCS SP5, Leica Microsystems) with Leica software (LAS AF LITE). An argon laser with absorption/fluorescence emission maxima at 499/520 nm and at 556/573 nm was used to detect fluorescent cells (maximum resolution: 4096 × 4096 pixels). Cell-counts were performed using a plug-in from Fiji (ImageJ). A Student's t-test was applied to compare the number of γ-pcdh ko versus wt cells. Values are expressed as mean ± SEM.

1. Wu, Q. & Maniatis, T. A striking organization of a large family of human neural cadherin-like cell adhesion genes. *Cell* **97**, 779–790 (1999).
2. Yagi, T. Clustered protocadherin family. *Dev Growth Differ* **50 Suppl 1**, (2008).
3. Kohmura, N. *et al.* Diversity revealed by a novel family of cadherins expressed in neurons at a synaptic complex. *Neuron* **20**, 1137–1151 (1998).
4. Murata, Y., Hamada, S., Morishita, H., Mutoh, T. & Yagi, T. Interaction with protocadherin-gamma regulates the cell surface expression of protocadherin-alpha. *J Biol Chem* **279**, 49508–49516 (2004).
5. Hambsch, B., Grinevich, V., Seeburg, P. H. & Schwarz, M. K. Gamma-Protocadherins, presenilin-mediated release of C-terminal fragment promotes locus expression. *J Biol Chem* **280**, 15888–15897 (2005).
6. Bonn, S., Seeburg, P. H. & Schwarz, M. K. Combinatorial expression of alpha- and gamma-protocadherins alters their presenilin-dependent processing. *Mol Cell Biol* **27**, 4121–4132 (2007).
7. Weiner, J. A., Wang, X., Tapia, J. C. & Sanes, J. R. Gamma protocadherins are required for synaptic development in the spinal cord. *Proc Natl Acad Sci U S A* **102**, 8–14 (2005).
8. Lefebvre, J. L., Zhang, Y., Meister, M., Wang, X. & Sanes, J. R. gamma-Protocadherins regulate neuronal survival but are dispensable for circuit formation in retina. *Development* **135**, 4141–4151 (2008).
9. Prasad, T., Wang, X., Gray, P. A. & Weiner, J. A. A differential developmental pattern of spinal interneuron apoptosis during synaptogenesis: insights from genetic analyses of the protocadherin-gamma gene cluster. *Development* **135**, 4153–4164 (2008).
10. Garrett, A. M., Schreiner, D., Lobas, M. A. & Weiner, J. A. gamma-Protocadherins Control Cortical Dendrite Arborization by Regulating the Activity of a FAK/PKC/MARCKS Signaling Pathway. *Neuron* **74**, 269–276 (2012).
11. Doetsch, F., Caille, I., Lim, D. A., Garcia-Verdugo, J. M. & Alvarez-Buylla, A. Subventricular zone astrocytes are neural stem cells in the adult mammalian brain. *Cell* **97**, 703–716 (1999).
12. Doetsch, F. A niche for adult neural stem cells. *Current Opinion in Genetics & Development* **13**, 543–550 (2003).
13. Temple, S. & Alvarez-Buylla, A. Stem cells in the adult mammalian central nervous system. *Current Opinion in Neurobiology* **9**, 135–141 (1999).
14. Kirschenbaum, B., Doetsch, F., Lois, C. & Alvarez-Buylla, A. Adult subventricular zone neuronal precursors continue to proliferate and migrate in the absence of the olfactory bulb. *Journal of Neuroscience* **19**, 2171–2180 (1999).
15. Petreanu, L. & Alvarez-Buylla, A. Maturation and death of adult-born olfactory bulb granule neurons: Role of olfaction. *Journal of Neuroscience* **22**, 6106–6113 (2002).
16. Whitman, M. C. & Greer, C. A. Synaptic integration of adult-generated olfactory bulb granule cells: basal axodendritic centrifugal input precedes apical dendrodendritic local circuits. *J Neurosci* **27**, 9951–9961 (2007).
17. Kelsch, W., Lin, C. W. & Lois, C. Sequential development of synapses in dendritic domains during adult neurogenesis. *Proc Natl Acad Sci U S A* **105**, 16803–16808 (2008).
18. Carleton, A., Petreanu, L. T., Lansford, R., Alvarez-Buylla, A. & Lledo, P. M. Becoming a new neuron in the adult olfactory bulb. *Nature Neuroscience* **6**, 507–51 (2003).
19. Wang, X. *et al.* Gamma protocadherins are required for survival of spinal interneurons. *Neuron* **36**, 843–854 (2002).
20. Li, Y. *et al.* Synaptic and nonsynaptic localization of protocadherin-gammaC5 in the rat brain. *J Comp Neurol* **518**, 3439–3463 (2010).
21. Veeraraghavalu, K., Choi, S. H., Zhang, X. & Sisodia, S. S. Presenilin 1 mutants impair the self-renewal and differentiation of adult murine subventricular zone-neuronal progenitors via cell-autonomous mechanisms involving notch signaling. *J Neurosci* **30**, 6903–6915 (2010).
22. Consiglio, A. *et al.* Robust in vivo gene transfer into adult mammalian neural stem cells by lentiviral vectors. *Proc Natl Acad Sci U S A* **101**, 14835–14840 (2004).
23. Jang, E. S. & Goldman, J. E. Pax6 expression is sufficient to induce a neurogenic fate in glial progenitors of the neonatal subventricular zone. *PLoS One* **6**, e20894 (2011).
24. Soriano, P. Generalized lacZ expression with the ROSA26 Cre reporter strain. *Nat Genet* **21**, 70–71 (1999).
25. Tanaka, S. *et al.* Interplay of SOX and POU factors in regulation of the Nestin gene in neural primordial cells. *Mol Cell Biol* **24**, 8834–8846 (2004).
26. Gotts, J. E. & Chesselet, M. F. Migration and fate of newly born cells after focal cortical ischemia in adult rats. *J Neurosci Res* **80**, 160–171 (2005).
27. Doetsch, F., GarciaVerdugo, J. M. & AlvarezBuylla, A. Cellular composition and three-dimensional organization of the subventricular germinal zone in the adult mammalian brain. *Journal of Neuroscience* **17**, 5046–5061 (1997).
28. Whitman, M. C. & Greer, C. A. Adult neurogenesis and the olfactory system. *Prog Neurobiol* **89**, 162–175 (2009).
29. Inta, D. *et al.* Neurogenesis and widespread forebrain migration of distinct GABAergic neurons from the postnatal subventricular zone. *Proc Natl Acad Sci U S A* **105**, 20994–20999 (2008).
30. Lemasson, M., Saghatelyan, A., Olivo-Marin, J. C. & Lledo, P. M. Neonatal and adult neurogenesis provide two distinct populations of newborn neurons to the mouse olfactory bulb. *J Neurosci* **25**, 6816–6825 (2005).
31. Clements, M. O. *et al.* Lentiviral manipulation of gene expression in human adult and embryonic stem cells. *Tissue Eng* **12**, 1741–1751 (2006).
32. Saura, C. A., Servian-Morilla, E. & Scholl, F. G. Presenilin/gamma-secretase regulates neurexin processing at synapses. *PLoS One* **6**, e19430 (2011).
33. Alberti, S. *et al.* Neuronal migration in the murine rostral migratory stream requires serum response factor. *Proceedings of the National Academy of Sciences of the United States of America* **102**, 6148–6153 (2005).
34. Andreu-Agullo, C., Morante-Redolat, J. M., Delgado, A. C. & Farinas, I. Vascular Niche Factor PEDF Modulates Notch-Dependent Stemness in Adult Neurogenic Niches. *Human Gene Therapy* **20**, 1026–1026 (2009).
35. Andreu-Agullo, C., Maurin, T., Thompson, C. B. & Lai, E. C. Ars2 maintains neural stem-cell identity through direct transcriptional activation of Sox2. *Nature* **481**, 195–198 (2012).
36. Lledo, P. M., Alonso, M. & Grubb, M. S. Adult neurogenesis and functional plasticity in neuronal circuits. *Nat Rev Neurosci* **7**, 179–193 (2006).
37. Doetsch, F., Garcia-Verdugo, J. M. & Alvarez-Buylla, A. Cellular composition and three-dimensional organization of the subventricular germinal zone in the adult mammalian brain. *J Neurosci* **17**, 5046–5061 (1997).

38. Lefebvre, J. L., Kostadinov, D., Chen, W. V., Maniatis, T. & Sanes, J. R. Protocadherins mediate dendritic self-avoidance in the mammalian nervous system. *Nature* **488**, 517–521 (2012).
39. Miyoshi, H., Blomer, U., Takahashi, M., Gage, F. H. & Verma, I. M. Development of a self-inactivating lentivirus vector. *J Virol* **72**, 8150–8157 (1998).
40. Dittgen, T. *et al.* Lentivirus-based genetic manipulations of cortical neurons and their optical and electrophysiological monitoring in vivo. *Proc Natl Acad Sci U S A* **101**, 18206–18211 (2004).
41. Pilpel, N., Landeck, N., Klugmann, M., Seeburg, P. H. & Schwarz, M. K. Rapid, reproducible transduction of select forebrain regions by targeted recombinant virus injection into the neonatal mouse brain. *J Neurosci Methods* **182**, 55–63 (2009).

Acknowledgements

The authors would like to thank Peter H. Seeburg for constant intellectual and financial support and Hannah Monyer for helpful advice during initial steps of the project. This work was supported by the Max Planck Society and grant SCHW 1578/1-1 by the DFG to M.K.S.

Author contributions

M.K.S. and J.L. designed the experiments, analyzed the results and wrote the manuscript. S.D. and J.L. performed the experiments.

Additional information

Supplementary information accompanies this paper at http://www.nature.com/scientificreports

Competing financial interests: The authors declare no competing financial interests.

How to cite this article: Ledderose, J., Dieter, S. & Schwarz, M.K. Maturation of postnatally generated olfactory bulb granule cells depends on functional γ-protocadherin expression. *Sci. Rep.* **3**, 1514; DOI:10.1038/srep01514 (2013).